Elastic full waveform inversion with probabilistic petrophysical model constraints

Odette Aragao & Paul Sava, Center for Wave Phenomena, Colorado School of Mines

SUMMARY

Accurate subsurface models of physical parameters are crucial for interpreting seismic data and understanding the subsurface geology. Wavefield tomography represents the state of the art technique used to derive models of elastic properties in seismic exploration and subsurface characterization. However, model updates provided by this methodology may not represent real lithologies in unconstrained multiparameter inversion. Petrophysical information provided by well logs can be incorporated into the inversion in order to constrain the inverted models to plausible solutions. We develop a method for elastic full waveform inversion that explicitly imposes petrophysical penalties to guide models toward realistic lithology, i.e., to models that are consistent with the seismic data as well as the underlying petrophysics. We achieve this goal by imposing feasible regions in the petrophysical space with probability density functions estimated from prior knowledge but without user-defined parameters. By using probabilistic model constraints, we avoid assuming explicit and potentially inaccurate petrophysical relations among the parameters. Using synthetic elastic examples, we demonstrate that probabilistic petrophysical constraints leads waveform inversion to models that are superior to models obtained either without such constraints or with approximate analytic constraints. Our methodology also reduces the potentially deleterious effects of the source radiation pattern, and of limited acquisition aperture.

INTRODUCTION

Full waveform inversion (FWI) is a wavefield tomography method that has the capacity to produce highly accurate subsurface models from seismic data (Tarantola, 1984; Pratt, 1999; Sirgue et al., 2004; Virieux and Operto, 2009). FWI iteratively updates model parameters according to the misfit between observed and simulated data. The inverse problem is solved by minimizing an objective function, whose gradient guides model updates that progressively decrease the data residual.

Initial implementations of FWI used the acoustic wave equation (Tarantola, 1984; Pratt, 1990; Pratt et al., 1996). However, elastic FWI better describes the subsurface properties (Tarantola, 1988; Pratt, 1990; Plessix, 2006), as acoustic wave propagation does not take into account elastic effects and the presence of S waves in the data. Elastic models are described by multiple parameters, including density ρ and Lamé parameters, λ and μ, or density and P- and S-wave velocities.

Despite the popularity FWI, many challenges hamper its routine, practical application. FWI is a highly nonlinear and ill-posed problem, so its convergence to an optimal solution is subjected to local minima (Symes, 2008; Virieux and Operto, 2009). Therefore, including prior information into the inversion is necessary to obtain reasonable solutions (Tikhonov and Arsenin, 1977; Tarantola, 2005).

Elastic FWI suffers from a number of additional practical difficulties. First, the inversion non-linearity increases when using multiple parameters (Operto et al., 2013). In addition, as model parameters are updated simultaneously but independently, different model components can be physically contradictory to one-another, creating combinations of model parameters that are lithologically implausible or impossible. This situation may lead to inaccurate and unstable wavefield simulations, and thus causes poor convergence (Baumstein, 2013). Moreover, similar radiation patterns controlled by various elastic parameters create crosstalk, i.e. one may not be able to differentiate between their impact on the data (Operto et al., 2013; Kamath and Tsvankin, 2016) resulting in infeasible models. Except for poorly illuminated areas, such crosstalk can be corrected by performing radiation pattern analysis.

Several works (Baumstein, 2013; Peters et al., 2015; Duan and Sava, 2016; Manukyan et al., 2018; Zhang et al., 2018; Rocha and Sava, 2018) show that model constraints imposed explicitly during inversion lead to recovered models that are consistent with the geologic understanding and properly characterize the subsurface. Petrophysical data, such as that derived from well logs, can be used to assemble these constraints. Geological constraints represent realistic lithological units by forcing the inverted models to be consistent with known physical relationships.

Duan and Sava (2016) and Rocha and Sava (2018) use a logarithmic penalty function that assumes a general linear relationship between the model parameters to constrain elastic wavefield tomography and elastic reflection waveform inversion, respectively. Both methodologies prove that this petrophysical constraint yields realistic models even if conventional regularization is not explicitly applied during the inversion. However, complex models may have a more complex, non-linear relationship between the elastic parameters. Moreover, the logarithmic penalty requires user-defined parameters, and their selection may be arduous, especially when different geological formations are present in the same area. Thus, it is necessary to define more general and automated petrophysical constraints that provide flexibility and exploit known information available from external sources (e.g., well logs).

We propose elastic full waveform inversion with an objective function that constrains the relationship between

the Lamé parameters λ and μ, using probability density functions (PDFs). We show that PDFs can be used in the definition of a penalty function for elastic FWI without defining an analytic relationship among the different elastic parameters. The performance of the proposed method is illustrated with a synthetic example.

ELASTIC WAVEFIELD TOMOGRAPHY

We consider the isotropic elastic wave equation

$$\rho\ddot{\mathbf{u}} - \lambda[\nabla(\nabla\cdot\mathbf{u})] - \mu\left[\nabla\cdot\left(\nabla\mathbf{u}+\nabla\mathbf{u}^T\right)\right] = \mathbf{f}, \quad (1)$$

where $\mathbf{u}(e,\mathbf{x},t)$ is the elastic wavefield, $\mathbf{f}(e,\mathbf{x},t)$ is the source function, $\lambda(\mathbf{x})$ and $\mu(\mathbf{x})$ are the Lamé parameters, $\rho(\mathbf{x})$ is the density and e, $\mathbf{x}$ and t are, respectively, the experiment index, space coordinates and time. Equation 1 assumes that Lamé parameters vary slowly, such that their spatial gradient can be neglected.

The inversion problem is solved by minimizing an objective function $\mathcal{J}(\mathbf{u}_s,\lambda,\mu)$ consisting of two parts: a term that calculates the misfit between the simulated and observed data $\mathcal{J}_D(\mathbf{u}_s,\lambda,\mu)$, and a term that imposes petrophysical model constraints.

We can define the data misfit term as

$$\mathcal{J}_D(\mathbf{u}_s,\lambda,\mu) = \sum_e \frac{1}{2}\left\|\mathbf{W}_u\mathbf{u}_s - \mathbf{d}_{obs}\right\|^2, \quad (2)$$

where $\mathbf{W}_u(e,\mathbf{x},t)$ are weights that restrict the source wavefield $\mathbf{u}_s(e,\mathbf{x},t)$ to the known receiver locations, and $\mathbf{d}_{obs}(e,\mathbf{x},t)$ are the observed data. We compute the gradient of $\mathcal{J}_D$ with respect to λ and μ using the adjoint-state method (Plessix, 2006), in order to update the model iteratively using gradient-based algorithms (Tarantola, 1988).

When one considers an objective function based solely on $\mathcal{J}_D$, the model components λ and μ are updated independently of one-another. Thus, they can become physically inconsistent with each other, producing subsurface models and consequently leading to inaccurate geologic interpretation. Explicitly incorporating petrophysical constraints improves the quality of the recovered models, as the constraints link the model parameters during the inversion, resulting in more accurate subsurface characterization.

Duan and Sava (2016) constrain the elastic full waveform inversion to a feasible region using a logarithmic penalty function $\mathcal{J}_L$, by using physical relationships between the updated model parameters:

$$\mathcal{J}_L(\lambda,\mu) = -\eta\sum_{\mathbf{x}}\left[\log\left(h_u\right)+\log\left(h_l\right)\right]. \quad (3)$$

The scalar parameter η determines the strength of the constraint term in the objective function, and h_u and h_l are linear functions that define, respectively, upper and lower boundaries of the feasible region:

$$h_u(\lambda,\mu) = -\lambda + c_u\mu + b_u, \quad (4)$$

$$h_l(\lambda,\mu) = +\lambda - c_l\mu - b_l. \quad (5)$$

The coefficients c_u and c_l are the slopes of the boundary lines, and b_u and b_l are their intercepts. The distance of a given model parameter in the parameter space $\{\lambda,\mu\}$ to the boundary lines h_u and h_l determines the strength of $\mathcal{J}_L$, such that this term dominates the objective function when models are close to either one of the barriers. This constraint forces the inverted models to move away from those boundaries, thus restricting them to a feasible region.

The term $\mathcal{J}_L$ assumes a linear relationship between the model parameters λ and μ, which may not be true for models with complex physical relationships. Considering that we have access to petrophysical information, such that obtained from well logs, we can impose a more general kind of petrophysical constraint. One can construct a model PDF using a normalized histogram of the reference well log parameters to characterize in a general, statistical sense, the dependence between the elastic model parameters.

For example, we could use a crossplot illustrating the petrophysical relationship between the Lamé parameters, λ and μ, to create a model PDF. For any given model with components (λ_x,μ_x), represented by the red dot in Figure 1, we would like to calculate a weighted distance to the entire distribution in the model parameter space. If this point is close to regions of high probability, the value of the petrophysical constraint $\mathcal{J}_P$ should be small. Otherwise, the value of $\mathcal{J}_P$ should be large and increasing when model parameters separate more from the distribution. To accomplish this, we construct a weighted sum of the distances between the model with (λ_x,μ_x) components to all other possible models in this space. The weight is proportional to the value of the PDF at a specific model cell and inverse proportional to the distance from the analyzed model to that cell.

The distance $d_x(i,j)$, in the model parameter space, from (λ_x,μ_x) to a cell with indices (i,j) is

$$d_x(i,j) = \sqrt{[\lambda(i)-\lambda_x]^2 + [\mu(j)-\mu_x]^2}, \quad (6)$$

for $i = 1\cdots N_\lambda$ and $j = 1\cdots N_\mu$ where N_λ and N_μ are the numbers of discrete intervals defined for parameters λ and μ, respectively. Then, the weight $w_x(i,j)$ from a specific model (λ_x,μ_x) to the cell at coordinates (i,j) with the probability density $P(i,j)$ is

$$w_x(i,j) = \frac{P(i,j)}{d_x(i,j)}. \quad (7)$$

The weighted distance $D_{\mathbf{x}}$ from the point (λ_x,μ_x) to the entire distribution is

$$D_{\mathbf{x}} = \sum_{i,j}\frac{P(i,j)}{d_x(i,j)}. \quad (8)$$

Using this process, we connect each point in the model parameter space to all other cells characterized by model

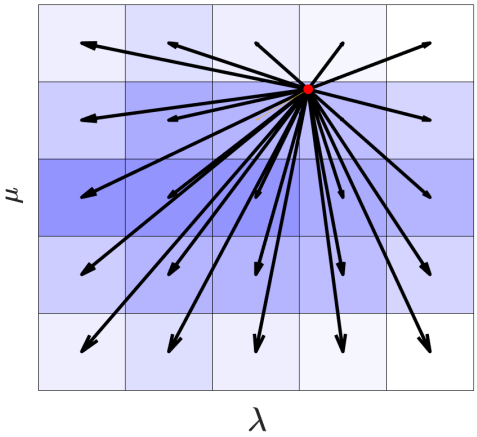

Figure 1: Sketch indicating how each point in the updated model parameter space (red dot) communicates with all cells of the model PDF. Each cell in the model parameter space contributes proportionally with its probability density value and inverse proportionally to the distance to the analyzed model.

PDF, i.e., we construct the distance from this model to the entire distribution. Since $D_{\mathbf{x}}$ is small for model cells that are far from regions of high probability, we can define $\mathcal{J}_P(\lambda,\mu)$ as

$$\mathcal{J}_P(\lambda,\mu) = \eta \sum_{\mathbf{x}} \frac{1}{D_{\mathbf{x}}}. \tag{9}$$

This definition imposes the condition that all points in the recovered models be as close as possible to the original petrophysical distribution without being drawn especially to any value in the model parameter space, but rather close to the region characterized by higher probability.

The gradient of $\mathcal{J}_P$ with respect to the model parameters λ and μ is

$$\begin{bmatrix} \frac{\partial \mathcal{J}_P}{\partial \lambda} \\ \frac{\partial \mathcal{J}_P}{\partial \mu} \end{bmatrix} = -\eta \begin{bmatrix} \left(\sum_{i,j} \frac{P(i,j)\,[\lambda(i)-\lambda_x]}{[d_x(i,j)]^3} \right) \sum_{i,j} \frac{1}{D_{\mathbf{x}}^2} \\ \left(\sum_{i,j} \frac{P(i,j)\,[\mu(j)-\mu_x]}{[d_x(i,j)]^3} \right) \sum_{i,j} \frac{1}{D_{\mathbf{x}}^2} \end{bmatrix}. \tag{10}$$

The value of $\mathcal{J}_P$ is determined by the distance to high probabilities in the model parameter space. Therefore, if the updated models are far from high probability, the gradient of $\mathcal{J}_P$ dominates in the total gradient of the objective function. Otherwise, this term smoothly forces the models away from regions of low probability.

The probabilistic petrophysical model constraint $\mathcal{J}_P$ addresses many relevant problems of elastic FWI. By incorporating prior information into the inversion, $\mathcal{J}_P$ reduces the non-linearity and ill-posed nature of FWI. Therefore, it reduces the number of possible model solutions and improves the inversion convergence. Additionally, by linking the elastic parameters during the inversion, it avoids geologically implausible earth models, and mitigates the artifacts created by interparameter crosstalk.

EXAMPLE

We illustrate our EFWI method with a synthetic example and compare inversions using (a) only the data misfit term $\mathcal{J}_D$, (b) the data misfit with the logarithmic penalty function $\mathcal{J}_D + \mathcal{J}_L$, and (c) the data misfit with the probabilistic petrophysical constraint $\mathcal{J}_D + \mathcal{J}_P$.

We use a portion of the Marmousi 2 model (Martin et al., 2002). Figure 2 shows the correct λ and μ models and the crossplot of the model parameters. We simulate a multicomponent ocean bottom seismic survey (OBS) with 20 evenly spaced pressure sources located at $z = 0.05$ km and a line of receiver at the water bottom ($z = 0.17$ km). We use a 7.5 Hz peak Ricker for the source signature. We compute the initial λ and μ models by repeatedly smoothing the true model. We consider that petrophysical data from three well logs are available. Figure 3 shows the well locations ($x = 1.1$, 2.0 and 3.0 km) and the crossplot of λ and μ models extracted at the wells. We use this information to build the penalties $\mathcal{J}_L$ and $\mathcal{J}_P$.

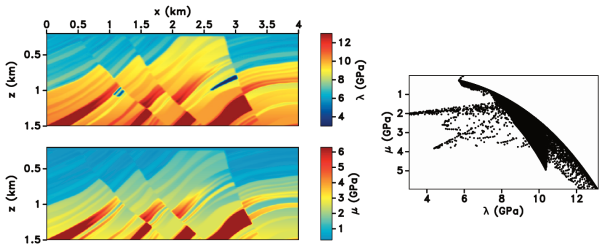

Figure 2: True λ and μ models and their crossplot.

Figure 4 shows the recovered λ and μ models using the objective function $\mathcal{J}_D$. The elastic parameter μ only depends on density and S-velocities, while λ depends on density as well as the P- and S-velocities. The S-wavelength is shorter than the P-wavelength, and therefore the inverted μ model has higher spatial resolution, and shows more structural detail than the recovered λ model. However, the μ model has spurious artifacts due to parameter crosstalk, that are not mitigated during the inversion in the absence of petrophysical constraints. Additionally, the crossplot shown in Figure 4 does not resemble the true model (Figure 2).

Figure 5 shows the recovered λ and μ models using the objective function $\mathcal{J}_D + \mathcal{J}_L$. The green lines in the crossplot corresponds to the upper and lower boundaries of the logarithmic penalty function that we estimate from the well logs ($+\lambda - 1.3\mu - 0.2 = 0$ and $-\lambda + 1.3\mu + 3.15 = 0$). We ensure that the starting models for inversion are within the feasible region. As for the preceding case (Figure 4), the inversion with linear

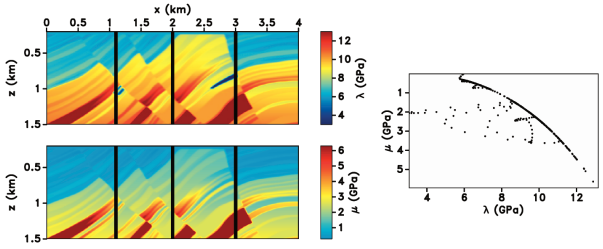

Figure 3: The vertical black lines correspond to well location that provide information for the petrophysical constraints. The crossplot of λ and μ derived from the well logs show that the relationship between the model parameters does not follow a simple trend.

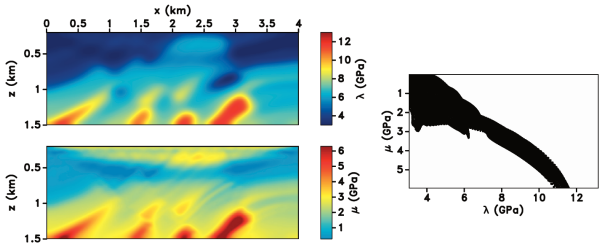

Figure 4: Recovered λ and μ models using objective function $\mathcal{J}_D$. The inverted μ model presents more structural details than the λ model.

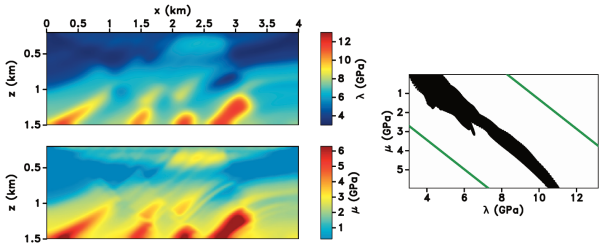

Figure 5: Recovered λ and μ models using objective function $\mathcal{J}_D + \mathcal{J}_L$. The lines overlain on the crossplot illustrate the upper and lower boundaries of the logarithmic penalty function $\mathcal{J}_L$.

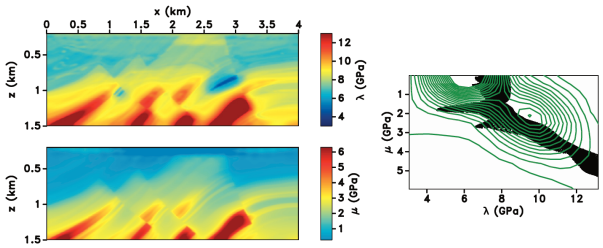

Figure 6: Recovered λ and μ models using objective function $\mathcal{J}_D + \mathcal{J}_P$. The contours overlain on the crossplot illustrate the feasible area used in the probabilistic penalty $\mathcal{J}_P$.

constraints can not alleviate interparameter crosstalk, so the inverted μ model has spurious artifacts. In addition, the crossplot shown in Figure 5 indicates that the logarithmic penalty function forces all recovered model towards the median between the barriers, although the linear boundaries do not correspond to the true models (Figure 2).

Figure 6 shows the recovered λ and μ models using the objective function $\mathcal{J}_D + \mathcal{J}_P$. The green contours correspond to the model PDF, which we estimate from the well log data without user-defined parameters. We also ensure that the initial model for inversion is within the feasible region, and the inverted λ and μ models shown in Figure 6 have similar resolution and are better recovered compared with the cases when we use the objective functions $\mathcal{J}_D$ (Figure 4) or $\mathcal{J}_D + \mathcal{J}_L$ (Figure 5). Additionally, the μ model artifacts caused by interparameter crosstalk are mitigated when we incorporate the probabilistic petrophysical constraints in the inversion. Also, note that the crossplot built with the inverted models (Figure 6) is closer to the similar crossplot built with the correct model parameters relative to the crossplots obtained for the unconstrained objective function $\mathcal{J}_D$ (Figure 4) or for the objective function $\mathcal{J}_D + \mathcal{J}_L$, that assumes an approximate analytic relationship between the elastic parameters (Figure 5).

CONCLUSIONS

We develop a strategy for incorporating petrophysical information, such as that provided by well logs, into elastic full waveform inversion through a penalty term using probability density functions. We demonstrate that imposing model petrophysical constraints improves the quality of the inverted subsurface models and better represents geologically plausible solutions, as the models are restricted to a feasible region during inversion. A synthetic example shows that, by using the proposed method, the recovered models are closer to the true models, while maintaining robust and realistic petrophysical relationships between the model parameters. In order to further enhance the geologic realism of models provided by elastic FWI, one can also include a spatial regularization term in the objective function.

ACKNOWLEDGMENTS

We acknowledge CAPES (Brazilian Federal Agency for Support and Evaluation of Graduate Education) for financial support. We thank the sponsors of the Center for Wave Phenomena (CWP), whose support made this research possible. The synthetic examples in this paper uses the Madagascar open-source software package (Fomel et al., 2013) freely available from http://www.ahay.org.

REFERENCES

Baumstein, A., 2013, POCS-based geophysical constraints in multiparameter full wavefield inversion: Presented at the 75th European Association of Geoscientists and Engineers Conference and Exhibition.

Duan, Y., and P. Sava, 2016, Elastic wavefield tomography with physical model constraints: Geophysics, **81**, no. 6, R447–R456.

Fomel, S., P. Sava, I. Vlad, Y. Liu, and V. Bashkardin, 2013, Madagascar: open-source software project for multidimensional data analysis and reproducible computational experiments: Journal of Open Research Software, 8th ed., DOI: http://dx.doi.org/10.5334/jors.ag.

Kamath, N., and I. Tsvankin, 2016, Elastic full-waveform inversion for VTI media: methodology and sensitivity analysis: Geophysics, **81**, no. 2, C53–C68.

Manukyan, E., H. Maurer, and A. Nuber, 2018, Improvements to elastic full-waveform inversion using cross-gradient constraints: Geophysics, **83**, no. 2, R105–R115.

Martin, G., K. Marfut, and S. Larsen, 2002, Marmousi-2, an updated model for the investigation of avo in structurally complex areas: Presented at the SEG Technical Program Expanded Abstracts.

Operto, S., Y. Gholami, V. Prieux, A. Ribodetti, R. Brossier, L. Metivier, and J. Virieux, 2013, A guided tour of multiparameter full-waveform inversion with multicomponent data: from theory to practice: The Leading Edge, **32**, no. 9, 1040–1054.

Peters, B., Z. Fang, B. R. Smithyman, and F. J. Herrmann, 2015, Regularizing waveform inversion by projections onto intersections of convex sets: Presented at the 77th European Association of Geoscientists and Engineers Conference and Exhibition.

Plessix, R. E., 2006, A review of the adjoint-state method for computing the gradient of a functional with geophysical applications: Geophysical Journal International, **167**, no. 2, 495–503.

Pratt, R. G., 1990, Inverse theory applied to multi-source cross-hole tomography: Geophysical Prospecting, **38**, 311–329.

———, 1999, Seismic waveform inversion in the frequency domain. Part 1: Theory and verification in a physical scale model: Geophysics, **64**, 888–901.

Pratt, R. G., Z. M. Williamson, and M. Warner, 1996, Two-dimensional velocity model from wide-angle seismic data by wavefield inversion: Geophysical Journal International, **124**, 323–340.

Rocha, D., and P. Sava, 2018, Elastic reflection waveform inversion with petrophysical model constrains: Presented at the SEG Technical Program Expanded Abstracts.

Sirgue, L., , and R. Pratt, 2004, Efficient waveform inversion and imaging: a strategy for selecting temporal frequencies: Geophysics, **69**, 231–248.

Symes, W. W., 2008, Migration velocity analysis and waveform inversion: Geophysical Prospecting, **56**, no. 6, 765–790.

Tarantola, A., 1984, Inversion of seismic reflection data in the acoustic approximation: Geophysics, **49**, 1259–1266.

———, 1988, Theoretical background for the inversion of seismic waveforms including elasticity and attenuation: Pure and Applied Geophysics, **128**, 365–399.

———, 2005, Inverse Problem Theory and Methods for Model Parameter Estimation: Society for Industrial and Applied Mathematics.

Tikhonov, A., and V. Arsenin, 1977, Solution of ill-posed problems: Winston and Sons.

Virieux, J., and S. Operto, 2009, An overview of full-waveform inversion in exploration geophysics: Geophysics, **74**, no. 6, WCC1–WCC26.

Zhang, Z., T. Alkhalifah, E. Z. Naeini, and B. Sun, 2018, multiparameter elastic full waveform inversion with facies-based constraints: Geophysical Journal International, **213**, 2112–2127.